

Article

A Simplified Method for the Evaluation of Floating-Body Motion Responses over a Sloping Bottom

Xiaolei Liu ^{1,2,*}, Kun Gu ¹, Zhijia Qian ³, Sheng Ding ², Kan Wang ^{1,*} , Hao Wang ¹ and Chen Sun ⁴

¹ College of Ocean Science and Engineering, Shanghai Maritime University, Shanghai 201306, China; 202330410145@stu.shmtu.edu.cn (K.G.); wanghao2@shmtu.edu.cn (H.W.)

² Central-Tech (Shanghai) Renewable Energy Technology Co., Ltd., Shanghai 200030, China; sheng.ding@groktech.com.cn

³ School of Marxism, Nanjing University of Finance and Economics, Nanjing 210023, China

⁴ Carbon Neutrality Research Center, State Power Investment Corporation Research Institute, Beijing 102209, China; sunchen@spic.com.cn

* Correspondence: liuxiaolei@shmtu.edu.cn (X.L.); wangk@shmtu.edu.cn (K.W.)

Abstract: Recently, many floating renewable energy platforms have been deployed in coastal regions, where sloping bottoms are an important factor when evaluating their safety. In this article, a simplified method coupling an eigenfunction matching method (EMM) and a finite-depth Green's function (FDGF) is developed to evaluate floating-body motion responses over a sloping bottom for which bathymetry is homogeneous in the longshore direction. We propose an extended EMM to create an incident wave model over the sloping bottom, thereby obtaining the Froude–Krylov (F–K) force and Neumann data on the wet surfaces of the floating body for the diffraction problem. An equivalent depth is introduced to account for the interaction between the sloping bottom and floating bodies when dealing with the diffraction and radiation problems. The accuracy of the present method is validated through a comprehensive comparison with numerical and/or experiment results for a liquefied natural gas (LNG) ship and a floating hemisphere from the literature. Generally, the present, simplified method can give predictions with sufficient accuracy.

Keywords: motion response; sloping bottom; simplified method; eigenfunction matching method; finite-depth Green's function



Citation: Liu, X.; Gu, K.; Qian, Z.; Ding, S.; Wang, K.; Wang, H.; Sun, C. A Simplified Method for the Evaluation of Floating-Body Motion Responses over a Sloping Bottom. *J. Mar. Sci. Eng.* **2024**, *12*, 756. <https://doi.org/10.3390/jmse12050756>

Academic Editor: Leszek Chybowski

Received: 5 March 2024

Revised: 23 April 2024

Accepted: 27 April 2024

Published: 30 April 2024



Copyright: © 2024 by the authors. Licensee MDPI, Basel, Switzerland. This article is an open access article distributed under the terms and conditions of the Creative Commons Attribution (CC BY) license (<https://creativecommons.org/licenses/by/4.0/>).

1. Introduction

Recently, more and more floating renewable energy facilities have been installed in coastal regions. For example: (1) China's first offshore floating PV station using ocean sun floats (water depth: 20–30 m) was set up in 2022 in the Chinese Yellow Sea (see Figure 1). (2) China's first floating offshore wind turbine, called “San Xia Yin Ling Hao” (water depth: approximately 28 m), was connected to the grid in 2021 in Yangjiang in South China's Guangdong province.

However, when a floating body is installed near shoreline and islands, the seabed's effects on the motion of the floating body become more significant than those for a deep water environment [1]. From the beginning of the 21st century, lots of ocean engineering experts have paid attention to motion responses of floating structures in nearshore areas. Their investigations show that large interaction has been found between the seabed and the response characteristics of floating structures, especially in low-wave-frequency ranges [2,3].

For hydrodynamic problems, water depth is always assumed to be constant when considering seabed effects. Hydrodynamic theories have been well established for both two-dimensional (2D) and three-dimensional (3D) problems. And scholars have developed corresponding numerical approaches, which can be divided into two types, i.e., analytical approaches and numerical approaches. For two-dimensional [4–6] and three-dimensional [7,8]

problems, analytical approaches (such as eigenfunction matching approaches) can be employed when the floating structure is of rectangular/cylindrical/spherical shape. In general, analytical approaches are always efficient, and their results have high accuracy, which means they can serve as benchmark solutions. While for hydrodynamic problems of arbitrary-geometry floating structures, numerical approaches are adopted due to their generality and flexibility. The boundary element method (BEM) is a specified numerical approach with a relatively small computational burden since all unknowns are distributed on the boundaries. Traditional surface-wave-body hydrodynamic problems using BEM always employ the finite-depth Green's function (FDGF), the evaluation of which is time-consuming since the function meets the demand of requiring partial boundary conditions. Different numerical techniques such as polynomial approximation [9,10] and power series expansions [11,12] have been developed to calculate this function and its partial derivatives. Corresponding commercial software [10,13] has been well-utilized in ocean engineering fields. Another BEM method, called the Rankine source approach, puts a simple green function on all the boundaries except for those in the far field, for which the numerical integral needs to be calculated. However, truncation of the numerical domain always introduces unwanted wave reflection from the artificial boundaries, which can be treated by specified techniques (see Feng et al. [2], Israeli and Orszag [14], Filippas and Belibassakis [15], Zhang and Beck [16], etc.).



Figure 1. China's first offshore floating PV station using ocean sun floats (water depth: 20–30 m).

However, when it comes to areas near the shoreline, the degree of seabed changes is significant with respect to the average water depth. Thus, previous methods using a constant depth assumption can no longer be applied. Analytical approaches have been developed to deal with this type of problem. For example, hydrodynamic wave loads of the floating body over sill on the bottom can be calculated [17], and this was further extended by Liu et al. [18] to a more general situation. To study the sloping seabed problem, a 2D Rankine source method with a novel source distribution strategy was brought up to eliminate the reflection from the truncated boundary [19].

To investigate 3D wave-body interactions over a sloping seabed, scholars have proposed some new numerical models. For instance, a very large floating structure (VLFS) can be divided into a number of small bodies, and their hydrodynamic responses are

solved by assuming every floating body is on a flat bottom with each local depth [20]. It should be pointed out that the researchers also assume a flat seabed for the far field in the circumferential direction. Another numerical model introduces a fixed underwater body to represent the undulating seabed [21,22]. However, the edge of the fixed body exerts a significantly irrational disturbance on the hydrodynamic responses [21], and an improved model by Hauteclocque et al. [23] was suggested to reduce the negative effects through introducing so-called transparent coefficients on the edges. Note that these coefficients are empirical and should be verified and corrected by experiments. Belibassakis [24] developed a new 3D BEM for the sloping seabed hydrodynamic problem by coupling a wave propagation model [25] and a sloping seabed Green's function [26]. However, Belibassakis [24]'s method requires the seabed to be smoothly varying, which is not in conformity with reality.

Moreover, a direct model coupling Boussinesq equations and the Rankine source method to solve the outer domain and the inner domain, respectively, was developed by Ding et al. [27] so as to include nonlinear wave effects. Similarly, Kim and Kim [28] developed a Rankine source method coupled with a numerical wave tank, in which a numerical damping zone is introduced by modifying the free surface boundary condition to avoid wave reflection in the far field. Their investigation using an LNG ship in moderate depths revealed that the main portion of wave loads is contributed by linear water waves. In addition, inhomogeneous waves are considered in Yang et al. [29]'s model to analyze the hydroelastic responses of a VLFS.

It can be seen that existing research about wave-body hydrodynamic interactions over a sloping seabed is insufficient. In order to carefully consider the effects of a sloping seabed with computational efficiency guaranteed, this article tries to develop a simplified method based on a wave propagation model and FDGF.

Scholars and experts in coastal engineering fields have set up various models [30–33] to treat wave propagation over a sloping seabed. Among these models, EMM [32] can deal with arbitrarily shaped seabeds, while a mild-slope equation assumes the seabed inclination to be small enough, and Athanassoulis and Belibassakis [25]'s model assumes a consistently varied seabed. EMM was employed in our previous research [34] to consider sloping seabed effects in a wave-body interaction problem in which the normal sea situation is considered. In this article, we further extend EMM into oblique incident wave problems. And it is obvious that EMM can provide accurate estimation of not only the Froude-Krylov force but also the Neumann data on the wet surface of the floating body for the diffraction problem.

Though the FDGF in terms of the constant water depth assumption does not permit its direct application in a sloping bottom problem, we believe that by introducing a proper choice of an equivalent depth h_e that is between the minimum and maximum depth of the bottom, one can obtain solutions with sufficient accuracy, as will be demonstrated later in this paper.

The differences between the present method and conventional commercial codes associated with finite-depth Green's function are threefold. The first one is that in the present method, EMM is applied to take the sloping bottom effects on incident wave potential into account. A second difference is that the Neumann data of boundary condition on the wet surface for the diffraction problem are provided by EMM, while the counterpart for conventional commercial codes is pre-given, which does not take the sloping bottom into account. The last one is the choice of the equivalent depth for the diffraction and radiation problems. As implementation of EMM is not difficult and evaluation methods for the finite-depth Green function have been established in many literature sources so far, it is expected that the present simplified method can provide an efficient way to treat this type of problem.

The rest of this paper is organized as follows: The mathematical model of a 3D hydrodynamic problem over a sloping bottom is formulated in Section 2. Section 3 gives a detailed description of the present, simplified method to treat the present problem. Then, in Section 4, accuracy of this present method is verified by comparing experimental and numerical results from the existing literature. Finally, Section 5 gives the conclusions of this article.

2. Governing Equations and Boundary Conditions

As shown in Figure 2, hydrodynamic responses of a floating structure over an undulating seabed are considered in this section. We use Cartesian coordinates (x, y, z) with a horizontal x -axis, upward z -axis and origin based on still water. An incident wave with angle θ propagates from left to right, with wave forces acting on the floating body. An arbitrarily one-dimensional (1D) varied seabed is assumed, since most bathymetric lines in coastal areas are straight in the y direction. The left and right semi-infinite bottoms are flat, and the undulating part lies between them. The varied depth is expressed as

$$h = \begin{cases} h_l & x < a \\ h_r & x > b \end{cases} \tag{1}$$

where h_l represents the depth of the left semi-infinite bottom, while h_r represents the depth of the right semi-infinite bottom.

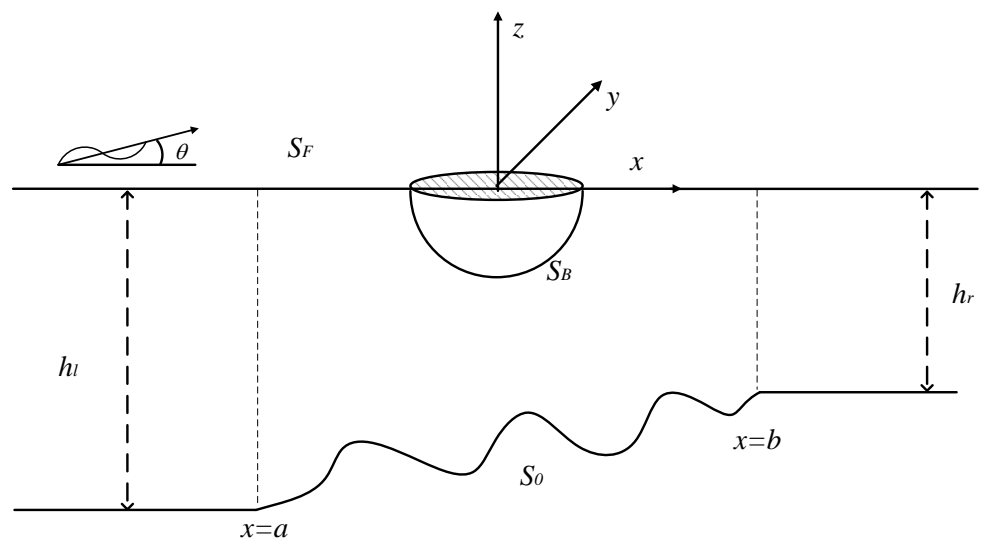


Figure 2. Wave–body hydrodynamic interaction over a sloping bottom.

S_0 , S_F and S_B denote the bottom, free water surface and wet surface of the floating body, respectively. An ideal fluid that is inviscid, incompressible and irrotational is assumed, and the amplitude a of the incident wave is small compared to the wavelength L ($a/L < 1/30$) [35]; therefore, nonlinear effects are neglected. The water depth is also small compared to L ($h_l/L < 0.5$) [35]; thus, the seabed exerts effects on the waves.

The governing equation of the velocity potential ϕ over the fluid domain is given by

$$\frac{\partial^2 \phi}{\partial x^2} + \frac{\partial^2 \phi}{\partial y^2} + \frac{\partial^2 \phi}{\partial z^2} = 0 \tag{2}$$

When incident wave ϕ_I acts on the floating body, the scattered wave field can be described by diffraction wave potential ϕ_D , while the forced oscillating body creates the radiation potential ϕ_R . All of the three potentials listed above must satisfy Equation (2).

On the still water surface, the wave potential gives

$$\frac{\partial \phi}{\partial z} - \frac{\omega^2}{g} \phi = 0 \quad (\text{on } S_F) \tag{3}$$

where ω and g represent the frequency and gravitational acceleration, respectively.

An impenetrable seabed condition gives (n denotes a unit normal vector on the seabed)

$$\frac{\partial \phi}{\partial n} = 0 \quad (\text{on } S_0) \tag{4}$$

For the diffraction problem, the body is assumed to be fixed, with the incident wave acting on the body; thus, the boundary condition on the wet surface is given by

$$\frac{\partial \phi_D}{\partial n} = -\frac{\partial \phi_I}{\partial n} \quad (\text{on } S_B), \text{ for diffraction problem} \tag{5}$$

On the other hand, for the radiation problem, the body is assumed to be experiencing forced oscillating motions v_b ; then, the boundary condition on the wet surface is given by

$$\frac{\partial \phi_R}{\partial n} = v_{bn} \quad (\text{on } S_B), \text{ for radiation problem} \tag{6}$$

where v_{bn} is the local velocity component on the boundary in the n direction, i.e., $v_{bn} = v_b \cdot n$.

3. A Simplified Method Combining the Eigenfunction Matching Method with the Finite-Depth Green’s Function

In this section, to analyze motion responses of floating bodies over a sloping bottom, a simplified method is established based on the EMM and FDGF. The EMM is extended to treat the problem of oblique propagation of water waves over a sloping seabed. For the diffraction and radiation solutions, effects of the sloping seabed are considered by introducing an equivalent depth, and the FDGF is still utilized.

3.1. Incident Wave Problem for Sloping Bottom Environment

Since the seabed is assumed to be 1D varied, the dimensionality of ϕ_I can be degraded [36] by

$$\phi_I(x, y, z) = e^{ik_y y} \varphi(x, z) \tag{7}$$

where $k_y = k_{11} \sin \theta$, and k_{11} can be solved by

$$k_{11} \tanh(k_{11} h_1) = \omega^2 / g \tag{8}$$

where k_{11} is the first eigenvalue (wave number) of the first rectangular subdomain $x \in (-\infty, a]$, and the first ‘1’ and the second ‘1’ represent the first subdomain and the first eigenvalue, respectively.

Thus, the corresponding 2D governing equation and boundary conditions are obtained

$$\frac{\partial^2 \varphi}{\partial x^2} + \frac{\partial^2 \varphi}{\partial z^2} - k_y^2 \varphi = 0 \tag{9}$$

$$\frac{\partial \varphi}{\partial z} - \frac{\omega^2}{g} \varphi = 0 \quad (\text{on } S_F) \tag{10}$$

$$\frac{\partial \varphi}{\partial n} = 0 \quad (\text{on } S_0) \tag{11}$$

According to the main idea of EMM, we approximate the sloping seabed into shelves with vertical steps, thus forming a list of rectangular subdomains. From Figure 3, it can be seen that the seabed is divided into M parts, and h_m represents the depth of the m -th rectangular subdomain $x \in (x_{m-1}, x_m]$, for which the incident wave potential is given:

$$\varphi = \begin{cases} \varphi_1 & x \in (-\infty, a], y \in (-\infty, \infty), z \in [-h_1, 0] \\ \varphi_m & x \in (x_{m-1}, x_m], y \in (-\infty, \infty), z \in [-h_m, 0] \\ \varphi_M & x \in [b, \infty), y \in (-\infty, \infty), z \in [-h_M, 0] \end{cases} \tag{12}$$

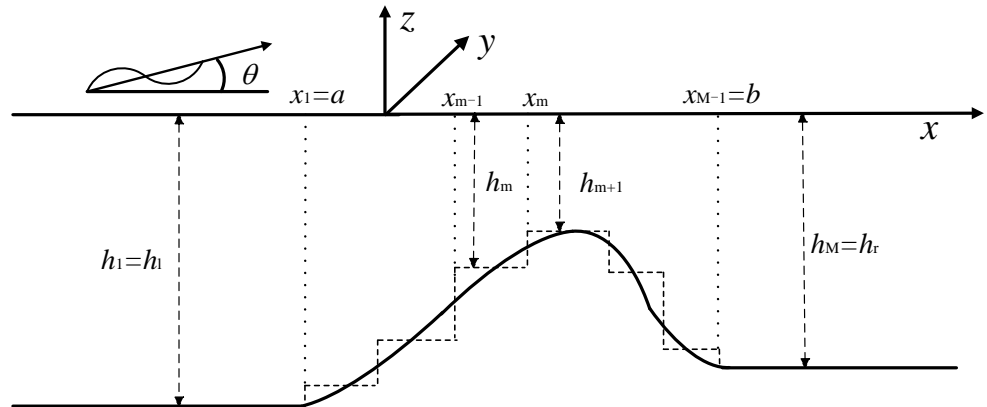


Figure 3. Approximation of the sloping seabed by shelves.

By eigenfunction expansion of Equation (9), the wave potential in the m -th subdomain is given by

$$\begin{aligned} \varphi_m = & [C_{m1}e^{i\sqrt{k_{m1}^2-k_y^2}(x-x_m)} + D_{m1}e^{-i\sqrt{k_{m1}^2-k_y^2}(x-x_{m-1})}]Z_{m,1} \\ & + \sum_{n=2}^{\infty} [C_{mn}e^{\sqrt{k_{mn}^2+k_y^2}(x-x_m)} + D_{mn}e^{-\sqrt{k_{mn}^2+k_y^2}(x-x_{m-1})}]Z_{m,n} \end{aligned} \tag{13}$$

where the first and remaining terms are the propagating eigenfunction and the evanescent eigenfunctions, respectively. $Z_{m,n}$ is the vertical expression of the n -th eigenfunction:

$$Z_{m,n} = \begin{cases} \cosh k_{m1}(z+h_m) / \cosh k_{m1}h_m & n = 1 \\ \cos k_{mn}(z+h_m) / \cos k_{mn}h_m & n = 2, 3, 4 \dots \end{cases} \tag{14}$$

where k_{mn} is obtained by solving the following equation:

$$\begin{cases} k_{m1} \tanh(k_{m1}h_m) = \omega^2/g \\ k_{mn} \tan(k_{mn}h_m) = -\omega^2/g \quad n = 2, 3, 4 \dots \end{cases} \tag{15}$$

On the interfaces between adjacent rectangular subdomains, the pressure and normal velocity should be consistent. For instance, at $x = x_m$, the following equations should be satisfied:

$$\varphi_m = \varphi_{m+1} \quad -h_{m+1} \leq z \leq 0 \tag{16}$$

$$\frac{\partial \varphi_m}{\partial x} = \begin{cases} \frac{\partial \varphi_{m+1}}{\partial x} & -h_{m+1} \leq z \leq 0 \\ 0 & -h_m \leq z < -h_{m+1} \end{cases} \tag{17}$$

Multiplying the above equations by $Z_{m,n}$ and integrating over the vertical interface, one has

$$\int_{-h_{m+1}}^0 \varphi_m Z_{m+1,n} dz = \int_{-h_{m+1}}^0 \varphi_{m+1} Z_{m+1,n} dz \quad n = 1, 2, 3, \dots \tag{18}$$

$$\int_{-h_m}^0 \frac{\partial \varphi_m}{\partial x} Z_{m,n} dz = \int_{-h_{m+1}}^0 \frac{\partial \varphi_{m+1}}{\partial x} Z_{m,n} dz \quad n = 1, 2, 3, \dots \tag{19}$$

By substituting Equation (13) into Equations (18) and (19), assuming n to be truncated to N , and having m vary from 1 to $M - 1$, then $2(M - 1)N$ linear equations are derived with $2MN$ unknowns, i.e., C_{mn} and D_{mn} .

In order to obtain solutions of the wave propagation problem, far field conditions give the remaining $2N$ linear equations, which are expressed as follows:

$$\begin{cases} C_{11} = -ig/\omega \\ D_{1n} = 0 \\ D_{M1} = 0 \\ C_{1n} = 0 \end{cases} \quad n = 2, 3, 4 \dots \tag{20}$$

3.2. Diffraction and Radiation Problems Considering the Sloping Seabed

By applying Green’s theorem, the boundary value problem for the diffraction and radiation potential can be solved by the following equations:

$$\frac{1}{2}\sigma(P) + \frac{1}{4\pi} \int_{S_B} \sigma(Q) \frac{\partial G}{\partial n(P)} dS = \frac{\partial \phi(P)}{\partial n(P)} \tag{21}$$

where P and Q are source points on the wet surfaces of floating bodies, G is Green’s function, σ is the source strength, and $\frac{\partial}{\partial n}$ denotes the normal partial derivative. And the wave potential $\phi(P)$ can be expressed as

$$\phi(P) = \frac{1}{4\pi} \int_{S_B} \sigma(Q) G dS \tag{22}$$

and

$$\frac{\partial \phi(P)}{\partial n(P)} = -\frac{\partial \phi_I}{\partial n} \quad (\text{on } S_B), \text{ for diffraction problem} \tag{23}$$

$$\frac{\partial \phi(P)}{\partial n(P)} = v_{bn} \quad (\text{on } S_B), \text{ for radiation problem} \tag{24}$$

A good choice for the Green’s function G is the bottom-dependent Green’s function of water waves over a sloping bottom connecting two flat bottoms developed by Belibassakis and Athanassoulis [26], as it automatically satisfies all the boundary conditions except for the wet surfaces. However, its calculation is quite cumbersome and time-consuming, which restricts its direct application.

In this study, we still employ the FDGF established by John [37], which can be expressed in the following form:

$$G = \frac{1}{r} + \frac{1}{r_2} + 2 \int_0^\infty \frac{(k + v) \cosh k(z + h_e) \cosh k(\zeta + h_e)}{k \sinh kh_e - v \cosh kh_e} e^{-kh} J_0(kR) dk \tag{25}$$

where G denotes the velocity potential at the field point (x, y, z) due to a point source at (ξ, η, ζ) , $v = \omega^2/g$, r is the distance between the source and field points, and r_2 is the distance between the field point and the image of the source point with respect to the bottom: here, an equivalent constant depth h_e is assumed to represent the contribution of the variable depth associated with the sloping seabed on the wave diffraction and radiation. Numerical methods for solving the finite-depth Green’s function have been fully studied elsewhere [10–12,33,38,39] and, thus, are not discussed here.

It is expected that solutions of the diffraction or radiation problem over a sloping bottom are between the results for the two constant water depths that denote the minimum and maximum depth of the bottom, i.e., h_{min} and h_{max} , respectively. Kim and Kim [28]’s results are associated with the radiation problem of an LNG ship have confirmed this assumption. With this in mind, one purpose of this study is to determine the equivalent constant depth h_e to represent a sloping seabed when analyzing wave diffraction and radiation to complete our simplified method.

After solving the problems above, incident, diffraction and radiation wave potentials are obtained. By using the Bernoulli equation and integrating it over the wet surface, the dynamic motion equations of the floating body are established:

$$(-\omega^2[M + A] - i\omega[B] + [K])\{\xi\} = \{f_w\} \tag{26}$$

where M is the mass matrix of the floating body, A is added mass, B is the damping coefficient, K is the hydro-static restoring matrix, and ζ and f_W are the complex amplitude of motion responses and wave exciting forces, respectively. Noted that one can refer to ref. [9] for the detailed derivation process of these physical quantities.

4. Results and Discussion

The numerical results for an LNG ship over mild-slope seabeds using the present method are shown and verified with the results of Hauteclocque et al. [23], Kim and Kim [28] and the experimental results of Buchner [21]. In order to demonstrate a broader range of this simplified method, comparisons are also made with the results of a floating hemisphere over a steep-slope bottom using a BEM method using a sloping seabed Green’s function [24]. Through these investigations, the equivalent depth is determined, and the accuracy of the present method is examined.

4.1. Comparison with Numerical Results for an LNG Ship

The motion response induced by an LNG ship over a sloping bottom is investigated here to show the accuracy of the simplified method. The length of the slope and the depths of two flat bottoms are designated as $L = 300$ m, $h_l = 30$ m and $h_r = 15$ m, respectively. The angle of the straight slope connecting the flat regions is $\arctan 1/20$, and it can be deemed to be a mild slope. The LNG ship is located at the center of the sloped bottom, the local water depth of which is 22.5 m. The size parameters of the LNG ship are given in Table 1.

Table 1. The LNG ship’s size parameters.

Parameter	Unit	Value
Length	m	274
Beam	m	44.2
Draft	m	11
Displacement	m ³	97120
Longitudinal center of gravity	m	−1.06 from midship
Vertical center of gravity	m	5.3 above still water plane
Roll radius of gyration	m	15.2
Pitch radius of gyration	m	68.5

Figures 4–6 show the predicted motion response amplitude operators (RAOs) of heave, pitch and surge calculated utilizing the present method with $h_e = 15, 22.5$ and 30 m and compared with the solutions from [28], who employed a numerical tank coupled with a Rankine source method, and the results from [23], who applied a new formulation of BEM with incident wave angle $\theta = 0$ deg. In Figure 4, the surge RAO using the present method with $h_e = 15$ and 22.5 m shows good agreement with numerical results [23] over almost all the frequencies. From Figures 5 and 6, it can be seen that the heave and pitch RAOs using the present method with $h_e = 22.5$ m exhibit close agreement with numerical solutions from the literature [23,28]. It seems that the present, simplified method with an equivalent depth corresponding to the local depth at the midship position can give accurate predictions of motion RAOs of the floating structure over a sloping seabed. This supposition can be further confirmed from Figure 7, which shows comparison of the heave RAO between the present method with $h_e = 15, 22.5$ and 30 m and the numerical results from Hauteclocque et al. [23] for an oblique wave $\theta = 15$ deg for an LNG ship. The heave RAO for an oblique wave using the present method with $h_e = 15$ and 22.5 m agrees well with the results from Hauteclocque et al. [23]. And the present method with $h_e = 15$ m shows good agreement, especially in the frequency range $0.6 \text{ rad/s} \leq \omega \leq 0.8 \text{ rad/s}$.

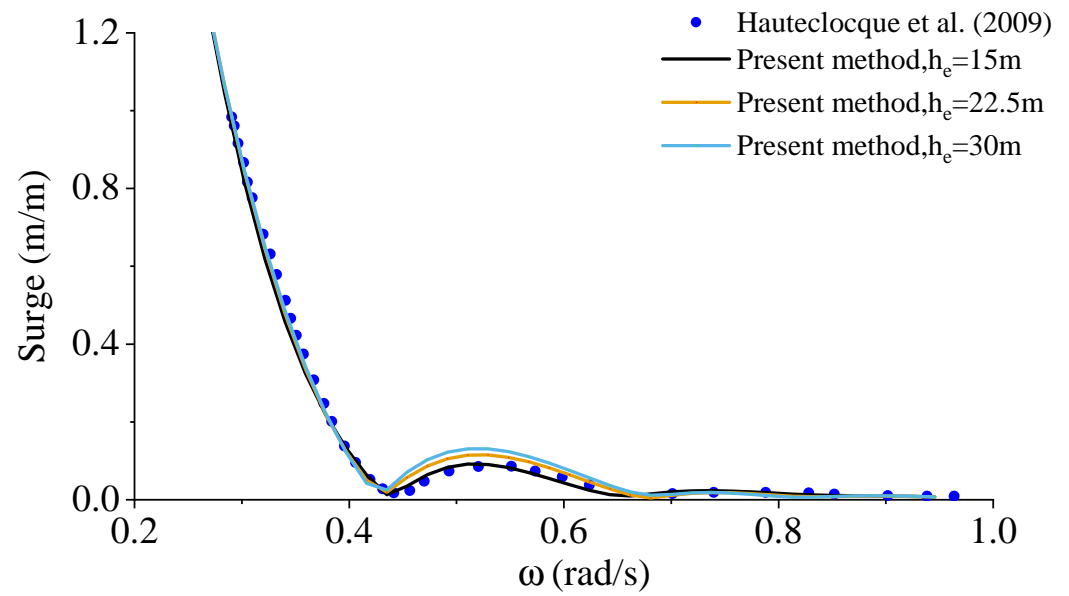


Figure 4. Comparison of surge RAOs between present method with $h_e = 15, 22.5$ and 30 m and solutions from Hauteclocque et al. [23] for incident wave with $\theta = 0$ deg for an LNG ship over a sloping seabed.

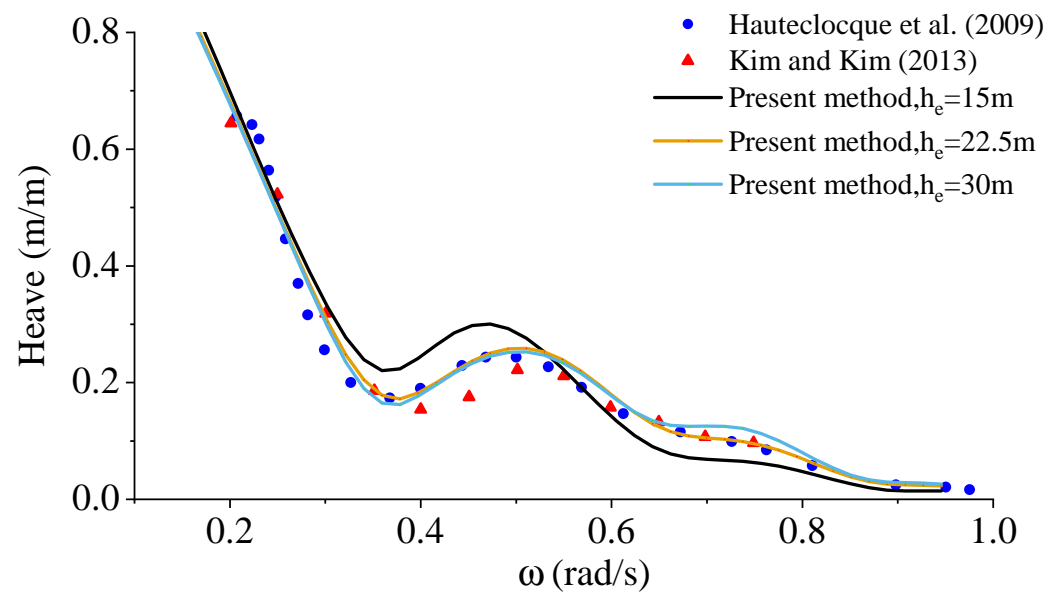


Figure 5. Comparison of heave RAOs between present method with $h_e = 15, 22.5$ and 30 m and numerical results from Hauteclocque et al. [23], Kim and Kim [28] for incident wave with $\theta = 0$ deg for an LNG ship over a sloping seabed.

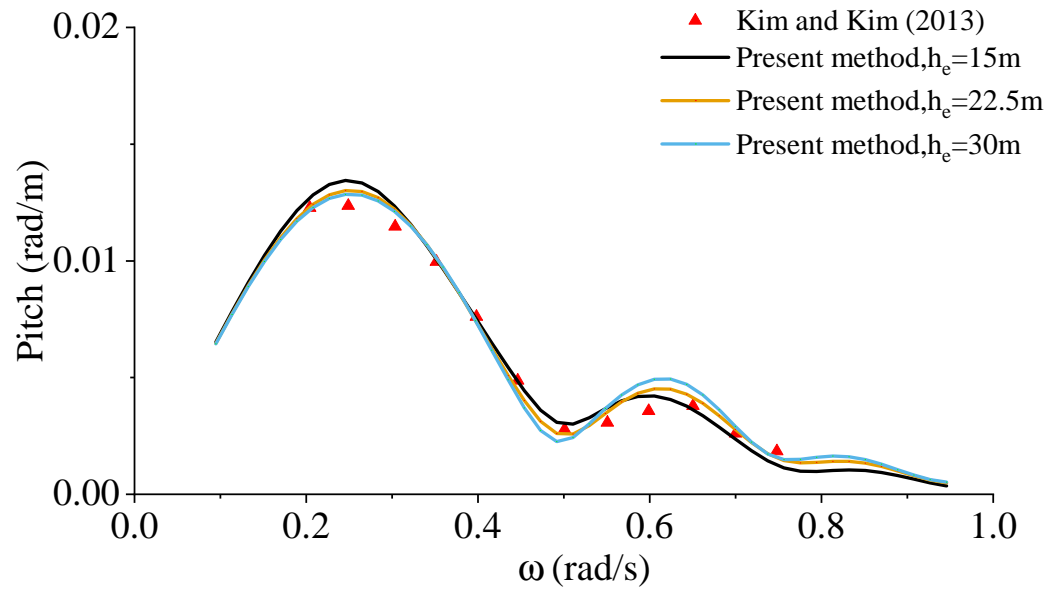


Figure 6. Comparison of pitch RAOs between present method with $h_e = 15, 22.5$ and 30 m and solutions from Kim and Kim [28] for incident wave with $\theta = 0$ deg for an LNG ship over a sloping seabed.

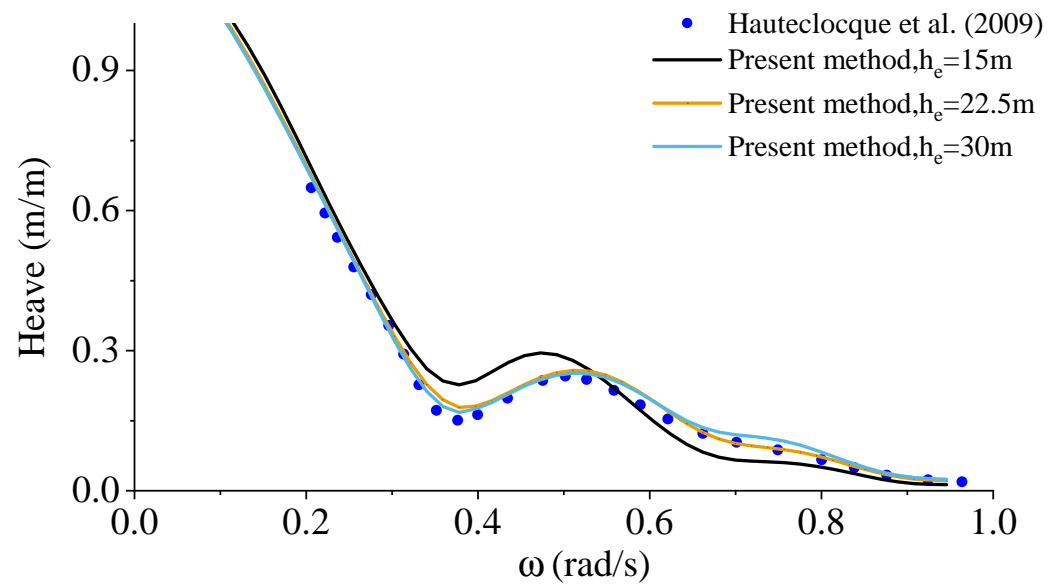


Figure 7. Comparison of heave RAOs between present method with $h_e = 15, 22.5$ and 30 m and solutions from Hauteclocque et al. [23] for an oblique wave with $\theta = 15$ deg for an LNG ship over a sloping seabed.

4.2. Comparison with Experimental Results for an LNG Ship

A model test of an LNG ship was carried out to investigate its motion responses over a sloping seabed by Buchner [21], and the main particulars of that LNG ship are the same as those used by Kim and Kim [28] and are given in Table 1. The author found that a method including a second fixed body is not possible (without special measures) when representing variable bathymetry using diffraction theory. In his model test, the normal water depth of the basin was 35 m. A wedge-type wooden straight slope with a sloping angle of $\arctan 1/20$ (mild slope) and a horizontal length of 550 m long was mounted on the flat bottom of the basin. With this slope, the water depth gradually decreased from 28 m at the bow to 21.5 m midship and 15 m at the stern of the LNG ship. We assume the position of midship to be at $x = 0$ m; thus, the starting and end points of the slope are at $x = -270$ m and $x = 280$ m, respectively.

Buchner [21] intended to model a sloping bottom connecting two flat bottoms, the depths of which were 35 m and 7.5 m, respectively, as shown in Figure 8a Slope I. However, we suggest that the model test is identical to Slope II (see Figure 8b) with an abrupt step at $x = 280$ m. In order to demonstrate this, both slopes are calculated using the present method and are compared with the experimental results from [21].

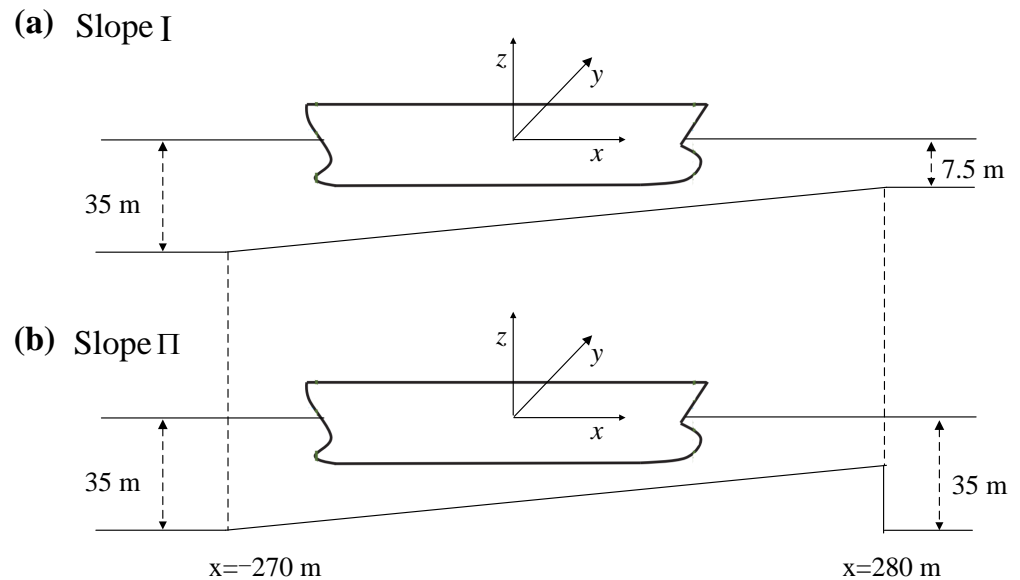


Figure 8. Configurations of the sloped bottom used to demonstrate a comparison with the experimental results from Buchner [21].

A comparison of pitch and heave motion RAOs between the present method with $h_e = 15, 21.5$ and 28 m over Slope I and the experimental results from Buchner [21] is illustrated in Figures 9 and 10, respectively. A slight difference between the curves of the pitch and heave motion RAOs using the present method with $h_e = 15, 21.5$ and 28 m is observed. A possible reason is that the dominant factor of problems associated with sloping bottoms is the characteristics of incident waves, i.e., the Froude–Krylov force and Neumann data on the wet surfaces of floating bodies for the diffraction problem. In this connection, differences between the results for different equivalent depth h_e values are not obvious; thus, we cannot tell which h_e gives better prediction results. Though the overall trends between the present method and the experimental results are similar, they agree well only in high-frequency regions, i.e., $\omega > 0.65$ rad/s for the pitch RAO and $\omega > 0.55$ rad/s for the heave RAO.

Figures 11 and 12 show a comparison for pitch and heave motion RAOs, respectively, between the present method with $h_e = 15, 21.5$ and 28 m over Slope II and the experimental results from Buchner [21]. For the pitch RAO, the results between the present method and the experimental results show good agreement except for a small region from 0.45 rad/s $< \omega < 0.6$ rad/s. And the heave RAO using the present method agrees well with the experiment results when $\omega > 0.55$ rad/s, while major differences occur in the low-frequency region. Note that the existence of the abrupt step at $x = 280$ m imposed a complex reflection of incident waves, leading to clear “wiggles” in the motion RAO curves using the present method (see Figures 11 and 12), which is also observed in the experimental results.

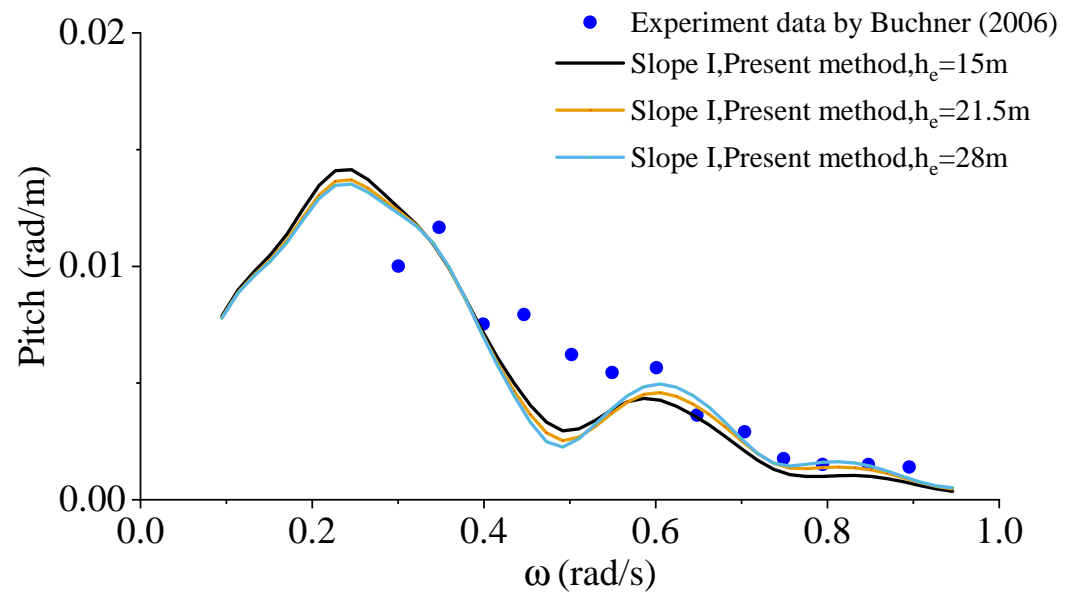


Figure 9. Comparison of pitch RAOs between present method with $h_e = 15, 21.5$ and 28 m over Slope I and experimental results from Buchner [21] for an incident wave with $\theta = 0$ deg for an LNG ship.

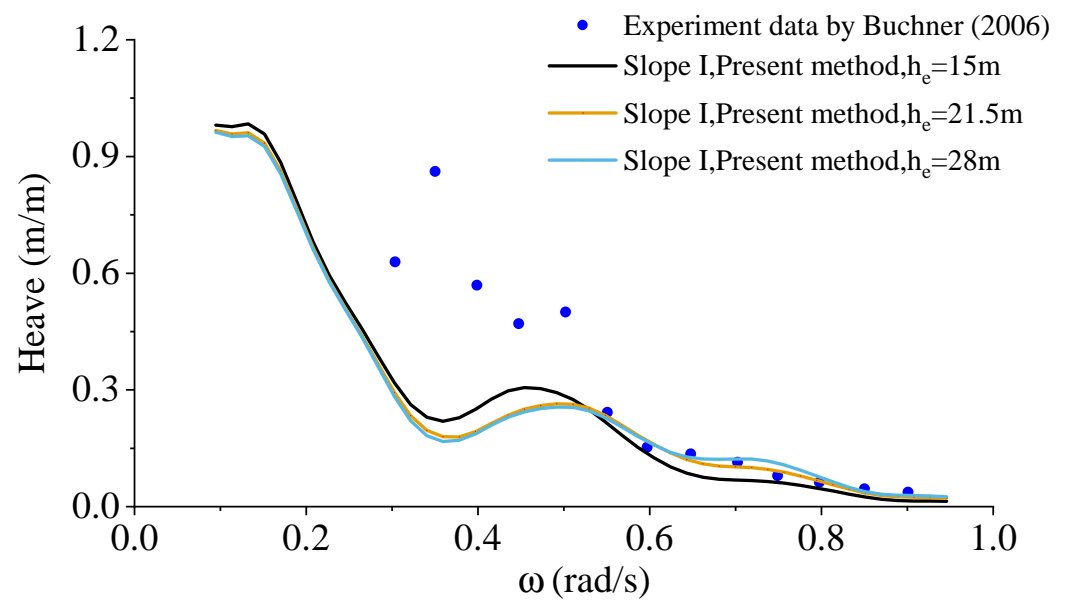


Figure 10. Comparison of heave RAOs between present method with $h_e = 15, 21.5$ and 28 m over Slope I and experimental results from Buchner [21] for an incident wave with $\theta = 0$ deg for an LNG ship.

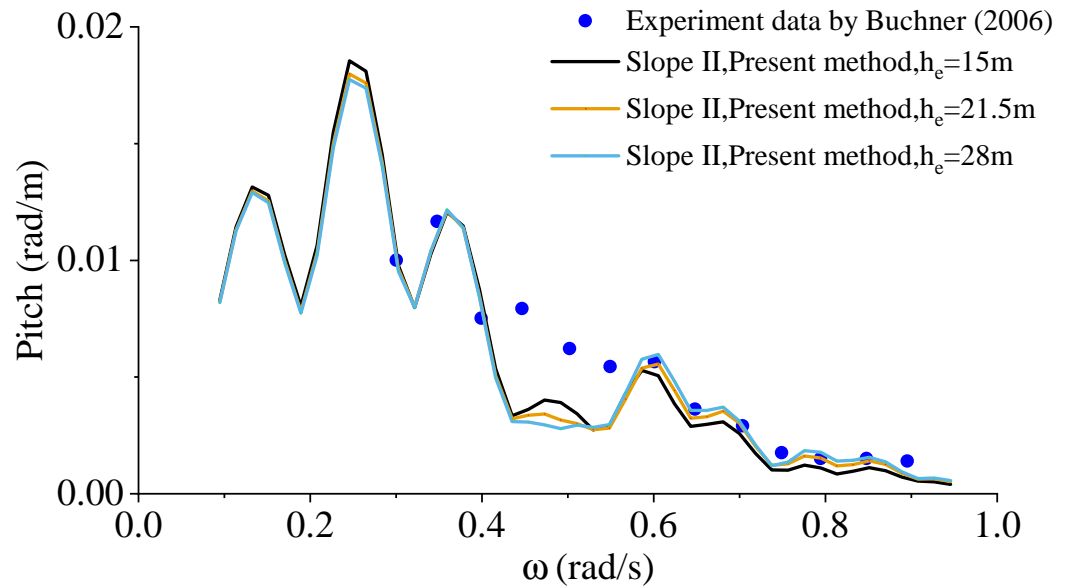


Figure 11. Comparison of pitch RAOs between present method with $h_e = 15, 21.5$ and 28 m over Slope II and experimental results from Buchner [21] for an incident wave with $\theta = 0$ deg for an LNG ship.

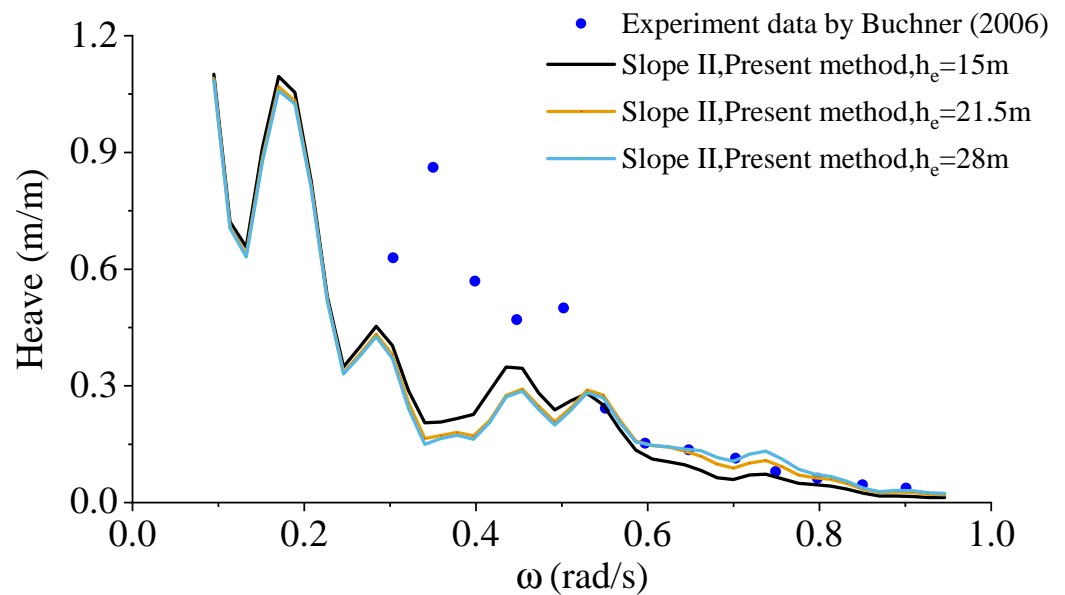


Figure 12. Comparison of heave RAOs between the present method with $h_e = 15, 21.5$ and 28 m over Slope II and experimental results from Buchner [21] for an incident wave with $\theta = 0$ deg for an LNG ship.

Taken together, these results suggest that Slope II is more suitable for representing the model test, and differences between the results of the present method with different h_e values are slight. In combination with the conclusion of the last subsection, we can infer that the present method with an equivalent depth h_e corresponding to the local depth midship can give accurate predictions of motion RAOs for an LNG ship over a mild-slope bottom.

4.3. Comparison with Numerical Results for a Floating Hemisphere

In the above subsections, comparisons of our method with published data related to LNG ships over mild-slope bottoms are shown. To expand the applicable scope of the present method, problems associated with a steep-slope bottom are considered in this part.

Recently, by using the boundary element method [24], we numerically investigated the effects of a sloping bottom on a floating hemisphere [40]. Note that Belibassakis [24]’s method assumes that $h(x)$ should be second-order continuous. And the $h(x)$ used by Liu et al. [40] is expressed as

$$h(x) = \frac{h_l + h_r}{2} - \frac{h_r - h_l}{2} \tanh 3\pi \left(\frac{x - a}{b - a} - \frac{1}{2} \right) \tag{27}$$

where $a = -10$ m and $b = 10$ m, and they are located at the start and end, respectively, of the sloping bottom areas. The water depths $h_l = 26$ m and $h_r = 14$ m are also assumed for the start and end of the slope, respectively; thus, the maximum slope of the bottom is 2.83, and the slope can be deemed to be very steep.

Table 2 gives the size parameters of the floating hemisphere, and it is located at the center of the sloping bottom at a local water depth of 20 m.

Table 2. The floating hemisphere’s size parameters.

Parameter	Unit	Value
Diameter	m	10
Displacement	m ³	261.8
Vertical center of gravity	m	0
Roll radius of gyration	m	3.16
Pitch radius of gyration	m	3.16
Yaw radius of gyration	m	3.16

Numerical simulations associated with the hemisphere over a sloping bottom for an incident wave angle $\theta = 0$ deg are shown in Figures 13 and 14. They show a comparison of the surge and heave RAOs between the present method with $h_e = 14, 20$ and 26 m and numerical results using Belibassakis [24]’s method. Firstly, it is observed that the results obtained using the present method with different h_e values are nearly identical, which further confirms our supposition that the dominant factor for problems associated with sloping bottoms is the velocity potential of the incident wave, which determines the F-K wave force and Neumann data for wave diffraction problems. Then, good agreement between the results using the present method and the method in the literature [24] further validates our method.

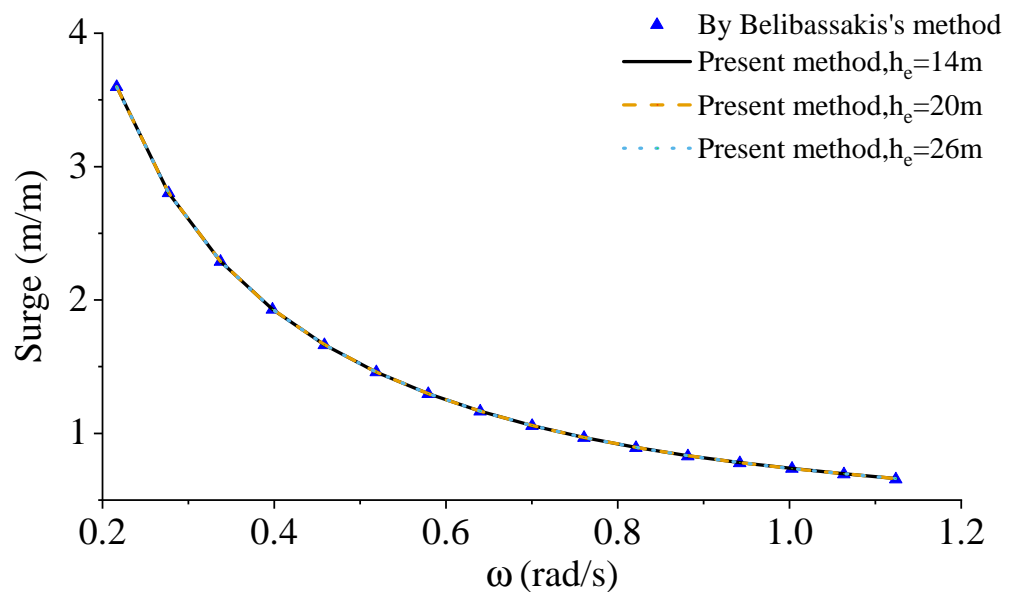


Figure 13. Comparison of surge RAOs between present method with $h_e = 14, 20$ and 26 m and numerical results using Belibassakis [24]’s method for incident wave with $\theta = 0$ deg for a hemisphere over an undulating seabed.

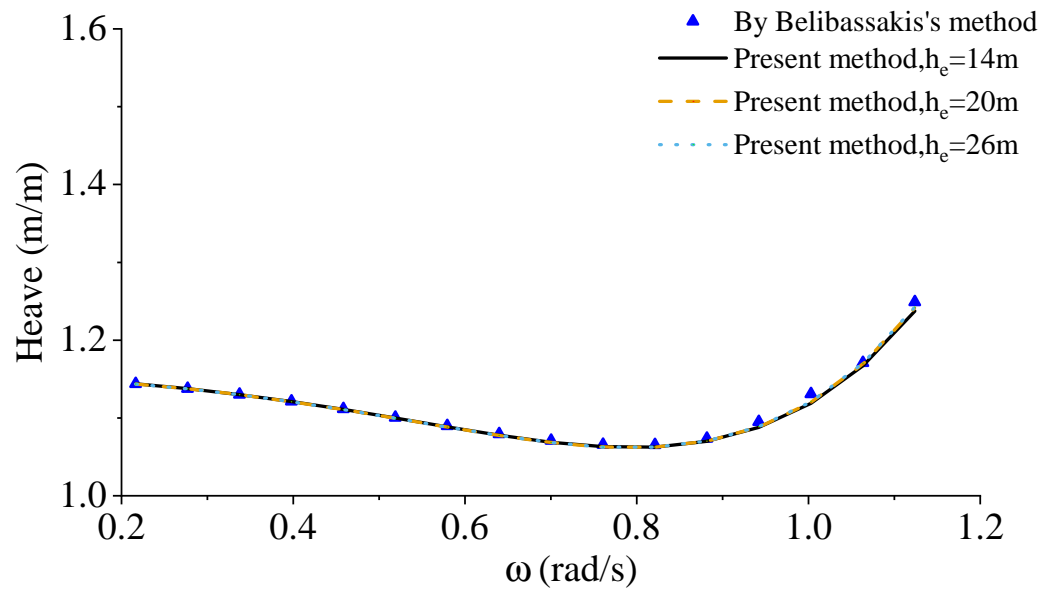


Figure 14. Comparison of heave RAOs between present method with $h_e = 14, 20$ and 26 m and numerical results using Belibassakis [24]’s method for an incident wave with $\theta = 0$ deg for a floating hemisphere over a sloping bottom.

Further numerical simulations are performed to validate the present method for oblique waves. Figures 15–17 show the comparison of surge, sway and heave RAOs between the present method with $h_e = 14, 20$ and 26 m and numerical results using Belibassakis [24]’s method for an oblique wave $\theta = 30$ deg for a floating hemisphere over a sloping bottom. Similar conclusions are deduced from these comparisons.

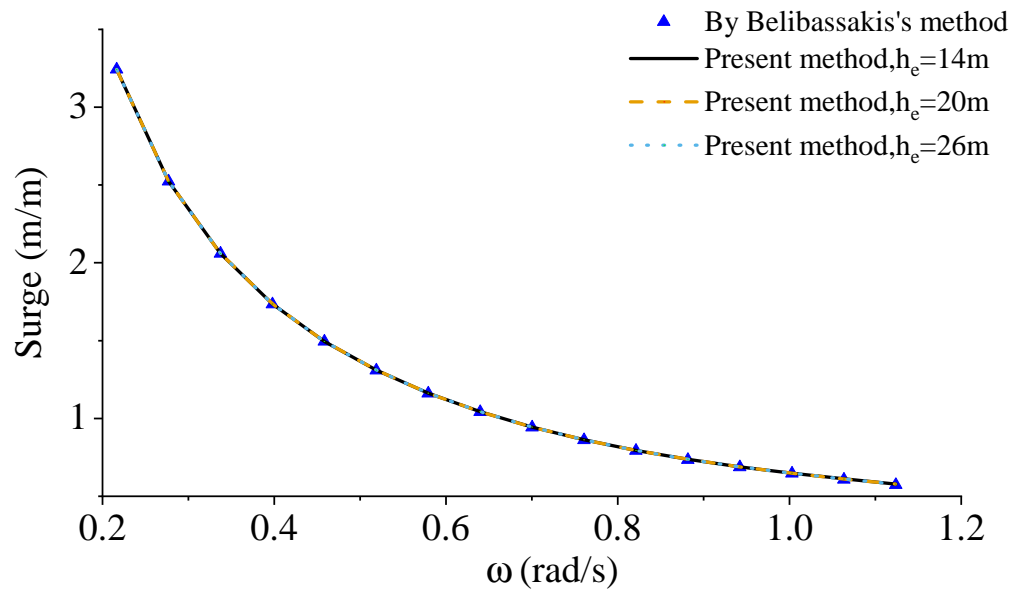


Figure 15. Comparison of surge RAOs between present method with $h_e = 14, 20$ and 26 m and numerical results using Belibassakis [24]’s method for an oblique wave with $\theta = 30$ deg for a hemisphere over an undulating seabed.

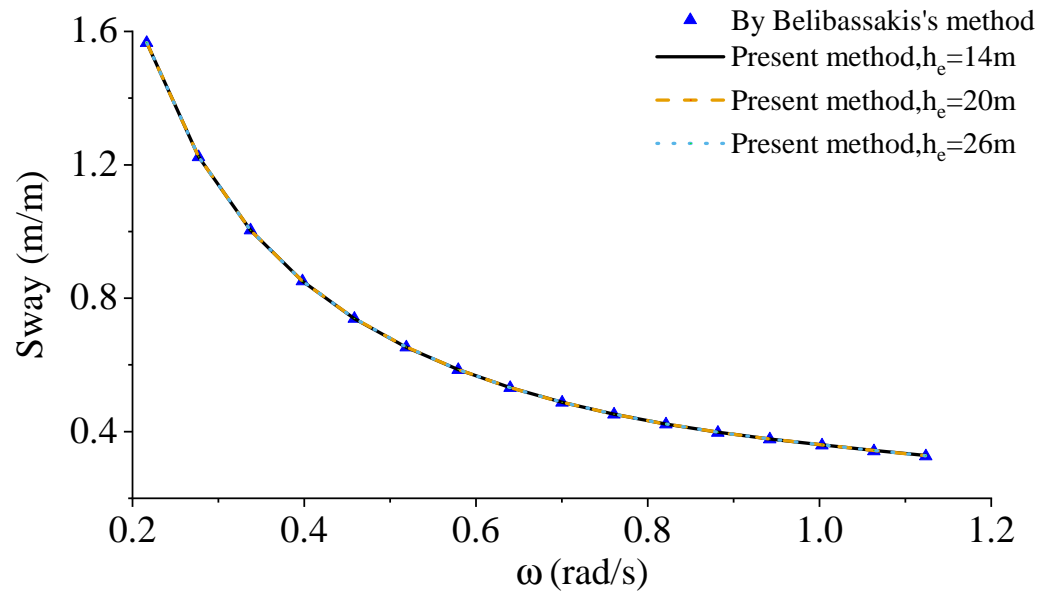


Figure 16. Comparison of sway RAOs between present method with $h_e = 14, 20$ and 26 m and numerical results using Belibassakis [24]’s method for an oblique wave with $\theta = 30$ deg for a hemisphere over an undulating seabed.

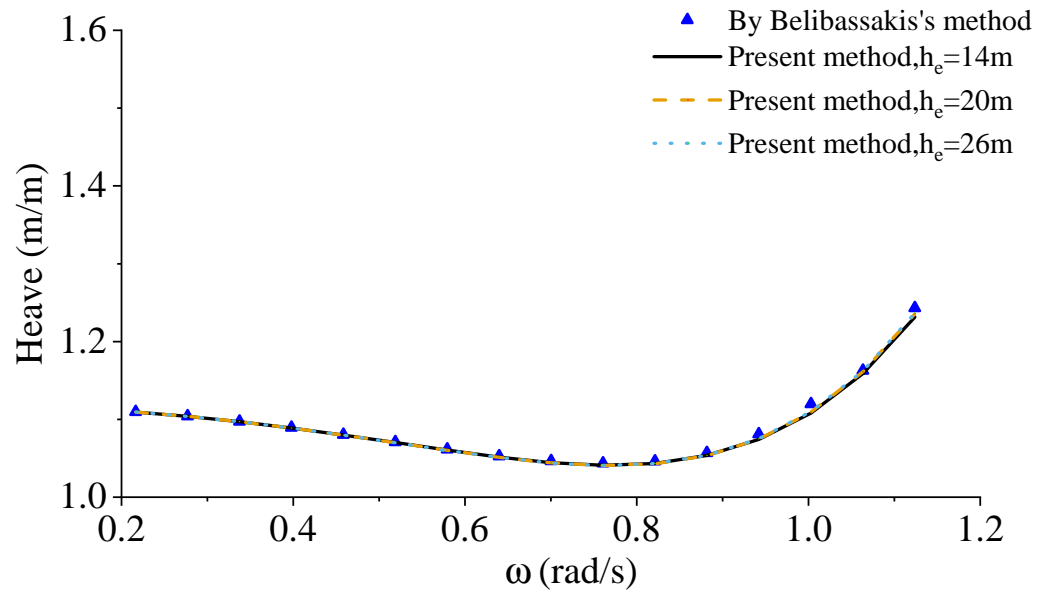


Figure 17. Comparison of heave RAOs between present method with $h_e = 14, 20$ and 26 m and numerical results using Belibassakis [24]’s method for an oblique wave with $\theta = 30$ deg for a hemisphere over an undulating seabed.

5. Conclusions

A simplified method combining the EMM with the FDGF is developed to study floating-body motion responses over a sloping seabed. An extended EMM is proposed to create an incident wave propagation model over a sloping bottom, with which the Froude–Krylov force and Neumann data on the wet surfaces of the floating body for the diffraction problem are obtained. Thus, the sloping bottom is carefully considered when solving the incident wave problem. In order to consider the effects of the undulating seabed for both wave diffraction and radiation, an equivalent depth between the minimum and maximum depths of the bottom is introduced, which indicates that a flat bottom is assumed when solving diffraction and radiation problems.

The accuracy of the present method is validated through some comparisons with numerical results and experimental data in the literature:

(1) For an LNG ship over a mild-slope bottom (a 300-meter-long slope), the present method with an h_e corresponding to the local depth midship agrees well with numerical results [23,28] for both normal and oblique waves. However, the differences between the results for the minimum and maximum depths of the bottom with data in the literature are relatively large. For the second mild-slope case (a 550-meter-long slope), the differences due to different h_e values are small, and the results using the present method agree well with the experimental results [21] except for at some frequency regions.

(2) Problems with respect to a hemisphere over a steep-slope bottom for both normal and oblique waves are further considered. The differences due to different h_e values between the minimum and maximum depths with the present method are not visible, and they agree well with the solutions using Belibassakis [24]'s approach.

In summary, the present, simplified method with an equivalent depth corresponding to the local depth midship can always give numerical results with sufficient accuracy.

Author Contributions: Conceptualization, X.L. and K.W.; methodology, X.L. and K.G.; software, X.L. and H.W.; validation, S.D. and H.W.; formal analysis, K.W.; investigation, X.L. and C.S.; resources, S.D.; data curation, K.W. and X.L.; writing—original draft preparation, K.W., X.L. and Z.Q.; writing—review and editing, S.D., X.L. and C.S.; visualization, K.G. and Z.Q.; supervision, X.L. and H.W.; project administration, K.W.; funding acquisition, K.W., S.D. and X.L. All authors have read and agreed to the published version of the manuscript

Funding: This research is funded by the National Natural Science Foundation of China (grant number 520011962) and is also funded as part of the research and development of key technologies for the transmission and application of medium- and low-pressure H2 and HCNG pipelines (grant number 2021ZD0038).

Institutional Review Board Statement: Not applicable.

Informed Consent Statement: Not applicable.

Data Availability Statement: The research data have been presented in the current paper.

Acknowledgments: The authors would like to express their sincere thanks to the editors and reviewers for their significant comments.

Conflicts of Interest: Author Xiaolei Liu is collaborating with the company Central-Tech (Shanghai) Renewable Energy Technology Co., Ltd. The remaining authors declare that the research was conducted in the absence of any commercial or financial relationships that could be construed as potential conflicts of interest.

Abbreviations

The following abbreviations are used in this manuscript:

h_l	Water depth of the left flat bottom
h_r	Water depth of the right flat bottom
ϕ	Wave velocity potential
ϕ_I	Incident wave potential
ϕ_D	Diffraction wave potential
ϕ_R	Radiation wave potential
ω	Wave frequency
g	Gravity acceleration
n	Unit normal vector
v_{bn}	Body velocity in the normal direction
k_{mn}	Eigenvalue of the dispersion relation
G	Green's function
σ	Source strength

h_e	Equivalent constant depth
r	Distance between the source and field points
r_2	Distance between the field point and the image of the source point
RAO	Response amplitude operator
BEM	Boundary element method
FDGF	Finite-depth Green's function
2D	Two-dimensional
3D	Three-dimensional
F-K	Froude–Krylov
EMM	Eigenfunction matching method

References

- Oortmerssen, G.V. The motions of a ship in shallow water. *Ocean Eng.* **1976**, *3*, 221–255. [[CrossRef](#)]
- Feng, A.; Tang, P.; You, Y.; Liu, K. Finite Water Depth Effect on Wave-Body Problems Solved by Rankine Source Method. *J. Ocean Univ. China* **2017**, *16*, 191–199. [[CrossRef](#)]
- Wang, Y.; Wang, X.; Xu, S.; Ding, A. Motion Response of a Moored Semi-Submersible-Type Single Module of a VLFS in Multi-Slope Shallow Water. *Int. J. Offshore Polar Eng.* **2017**, *27*, 397–405. [[CrossRef](#)]
- Zheng, Y.H.; You, Y.G.; Shen, Y.M. On the radiation and diffraction of water waves by a rectangular buoy. *Ocean Eng.* **2004**, *31*, 1063–1082. [[CrossRef](#)]
- Zheng, Y.; Shen, Y.; You, Y.; Wu, B.; Jie, D. On the radiation and diffraction of water waves by a rectangular structure with a sidewall. *Ocean Eng.* **2004**, *31*, 2087–2104. [[CrossRef](#)]
- Yang, X.-Y.; Zhang, H.-S.; Li, H.-T. Wave radiation and diffraction by a floating rectangular structure with an opening at its bottom in oblique seas. *J. Hydrodyn.* **2017**, *29*, 1054–1066. [[CrossRef](#)]
- Wu, B.-J.; Zheng, Y.-H.; You, Y.-G.; Sun, X.-Y.; Chen, Y. On diffraction and radiation problem for a cylinder over a caisson in water of finite depth. *Int. J. Eng. Sci.* **2004**, *42*, 1193–1213. [[CrossRef](#)]
- Hulme, A. The wave forces on a floating hemisphere undergoing forced periodic oscillations. *J. Fluid Mech.* **1982**, *121*, 443–463. [[CrossRef](#)]
- Newman, J.N. Algorithms for the free-surface Green function. *J. Eng. Math.* **1985**, *19*, 57–67. [[CrossRef](#)]
- Chen, X.B. Hydrodynamics in offshore and naval applications-Part I. In Proceedings of the Keynote Lecture of 6th International Conference on Hydrodynamics, Perth, WA, Australia, 24–26 November 2004.
- Linton, C. Rapidly convergent representations for Green's functions for Laplace's equation. *Proc. R. Soc. Lond. Ser. A Math. Phys. Eng. Sci.* **1999**, *455*, 1767–1797. [[CrossRef](#)]
- Liu, Y.; Iwashita, H.; Hu, C. A calculation method for finite depth free-surface green function. *Int. J. Nav. Archit. Ocean Eng.* **2015**, *7*, 375–389. [[CrossRef](#)]
- Lee, C.H. *WAMIT Theory Manual*; Massachusetts Institute of Technology, Department of Ocean Engineering: Cambridge, MA, USA, 1995.
- Israeli, M.; Orszag, S.A. Approximation of radiation boundary conditions. *J. Comput. Phys.* **1981**, *41*, 115–135. [[CrossRef](#)]
- Filippas, E.S.; Belibassakis, K.A. Hydrodynamic analysis of flapping-foil thrusters operating beneath the free surface and in waves. *Eng. Anal. Bound. Elem.* **2014**, *41*, 47–59. [[CrossRef](#)]
- Zhang, X.; Beck, R.F. Computations for large-amplitude two-dimensional body motions. *J. Eng. Math.* **2007**, *58*, 177–189. [[CrossRef](#)]
- Shen, Y.M.; Zheng, Y.H.; You, Y.G. On the radiation and diffraction of linear water waves by a rectangular structure over a sill. Part I. Infinite domain of finite water depth. *Ocean Eng.* **2005**, *32*, 1073–1097. [[CrossRef](#)]
- Liu, X.; Wang, X.; Xu, S.; Ding, A. Influences of a varying sill at the seabed on two-dimensional radiation of linear water waves by a rectangular buoy. *J. Offshore Mech. Arct. Eng.* **2020**, *142*, 041202. [[CrossRef](#)]
- Feng, A.; Bai, W.; Price, W.G. Two-dimensional wave radiation and diffraction problems in a flat or sloping seabed environment. *J. Fluids Struct.* **2017**, *75*, 193–212. [[CrossRef](#)]
- Murai, M.; Inoue, Y.; Nakamura, T. The prediction method of hydroelastic response of VLFS with sea bottom topographical effects. In Proceedings of the Thirteenth International Offshore and Polar Engineering Conference, Honolulu, HI, USA, 25–30 May 2003.
- Buchner, B. The Motions of a Ship on a Sloped Seabed. In Proceedings of the 25th International Conference on Offshore Mechanics and Arctic Engineering, Hamburg, Germany, 4–9 June 2006; pp. 339–347.
- Ferreira, M.; Newman, J. Diffraction effects and ship motions on an artificial seabed. In Proceedings of the 24th International Workshop on Water Waves and Floating Bodies, Zelenogorsk, Russia, 19–22 April 2009.
- Hauteclouque, G.D.; Rezende, F.; Giorgiutti, Y.; Chen, X.B. Wave Kinematics and Seakeeping Calculation With Varying Bathymetry. In Proceedings of the ASME 2009 28th International Conference on Ocean, Offshore and Arctic Engineering, Honolulu, HI, USA, 31 May–5 June 2009.
- Belibassakis, K.A. A boundary element method for the hydrodynamic analysis of floating bodies in variable bathymetry regions. *Eng. Anal. Bound. Elem.* **2008**, *32*, 796–810. [[CrossRef](#)]

25. Athanassoulis, G.A.; Belibassakis, K.A. A consistent coupled-mode theory for the propagation of small-amplitude water waves over variable bathymetry regions. *J. Fluid Mech.* **1999**, *75*, 275–301. [[CrossRef](#)]
26. Belibassakis, K.A.; Athanassoulis, G.A. Three-dimensional Green's function for harmonic water waves over a bottom topography with different depths at infinity. *J. Fluid Mech.* **2004**, *510*, 267–302. [[CrossRef](#)]
27. Ding, J.; Tian, C.; Wu, Y.S.; Li, Z.W.; Ling, H.J.; Ma, X.Z. Hydroelastic analysis and model tests of a single module VLFS deployed near islands and reefs. *Ocean Eng.* **2017**, *144*, 224–234. [[CrossRef](#)]
28. Kim, T.; Kim, Y. Numerical analysis on floating-body motion responses in arbitrary bathymetry. *Ocean Eng.* **2013**, *62*, 123–139. [[CrossRef](#)]
29. Yang, P.; Li, Z.; Wu, Y.; Wen, W.; Ding, J.; Zhang, Z. Boussinesq-Hydroelasticity coupled model to investigate hydroelastic responses and connector loads of an eight-module VLFS near islands in time domain. *Ocean Eng.* **2019**, *190*, 106418. [[CrossRef](#)]
30. Roseau, M. *Asymptotic Wave Theory*; Elsevier: Amsterdam, The Netherlands, 2012; Volume 20.
31. Berkhoff, J. Computation of combined refraction—Diffraction. In Proceedings of the 13th International Conference on Coastal Engineering, Vancouver, BC, Canada, 10–14 July 1972.
32. Kirby, J.T. A general wave equation for waves over rippled beds. *J. Fluid Mech.* **1986**, *162*, 171–186. [[CrossRef](#)]
33. Newman, J. Propagation of water waves over an infinite step. *J. Fluid Mech.* **1965**, *23*, 399–415. [[CrossRef](#)]
34. Liu, X.; Wang, X.; Xu, S. A DMM-EMM-RSM hybrid technique on two-dimensional frequency-domain hydroelasticity of floating structures over variable bathymetry. *Ocean Eng.* **2020**, *201*, 107135. [[CrossRef](#)]
35. Zou, Z. *Water Wave Theories and Their Applications*; Chinese Science Press: Beijing, China, 2005.
36. Massel, S.R. Extended refraction-diffraction equation for surface waves. *Coast. Eng.* **1993**, *19*, 97–126. [[CrossRef](#)]
37. John, F. On the motion of floating bodies II. Simple harmonic motions. *Commun. Pure Appl. Math.* **1950**, *3*, 45–101. [[CrossRef](#)]
38. Yang, P.; Gu, X.; Tian, C.; Cheng, X.; Ding, J. Numerical study of 3D pulsating source green function of finite water depth. In Proceedings of the ASME 2014 33rd International Conference on Ocean, Offshore and Arctic Engineering, American Society of Mechanical Engineers Digital Collection, San Francisco, CA, USA, 8–13 June 2014.
39. Liu, Y.; Cong, P.; Gou, Y.; Yoshida, S.; Kashiwagi, M. Enhanced Endo's approach for evaluating free-surface Green's function with application to wave-structure interactions. *Ocean Eng.* **2020**, *207*, 107377. [[CrossRef](#)]
40. Liu, X.; Wang, Y.; Wang, X.; Wang, L.; Miao, Q. Numerical investigation on motion responses of a floating hemisphere over a sloping bottom. *J. Offshore Mech. Arct. Eng.* **2021**, *143*, 051903. [[CrossRef](#)]

Disclaimer/Publisher's Note: The statements, opinions and data contained in all publications are solely those of the individual author(s) and contributor(s) and not of MDPI and/or the editor(s). MDPI and/or the editor(s) disclaim responsibility for any injury to people or property resulting from any ideas, methods, instructions or products referred to in the content.